Hindawi
International Journal of Aerospace Engineering
Volume 2023, Article ID 5541378, 10 pages
https://doi.org/10.1155/2023/5541378

Research Article

Velocity-Adaptive Prescribed Performance Control for Carrier-Based Aircraft Based on Guardian Maps

Chenliang Li, Jizhou Lai, Boyi Chen, and Yanbin Liu

Nanjing University of Aeronautics and Astronautics, Nanjing 210016, China

Correspondence should be addressed to Boyi Chen; cby_1989@126.com

Received 26 April 2023; Revised 31 July 2023; Accepted 9 August 2023; Published 31 August 2023

Academic Editor: Jiaqiang E

The automatic carrier landing process is a significant and complex due to the plant variation of carrier-based aircraft. To reasonably identify the stability interval for specific performance, an adaptive control strategy based on the guardian map approach is proposed. Prescribed performance, namely, stability margin, damping requirements, or flying quality requirements, is analytically formulated using a guardian map. The null space of guardian maps restricts the prescribed performance regarding the poles' location. The feasible corridor of control parameters is generated based on the null space of guardian maps. Besides, a velocity-adaptive prescribed performance control method is proposed to conduct the attitude control of carrier-based aircraft. Simulation shows that the short-period mode of carrier-based aircraft will be driven from unstable to stable as the velocity decreases. Moreover, simulation results demonstrate the proposed control method and indicate that the attitude loop control of carrier-based aircraft possesses more underdamped responses as the velocity decreases.

1. Introduction

Carrier-based aircraft (CA) are important naval air forces in modern navies. Short-distance take-off and landing ability are the critical concern. The aircraft should tightly follow the glideslope with a specific speed profile, then accurately land at the designated location with specific closed-loop performance [1]. Many undesirable landing conditions lead to the complex automatic carrier landing system (ACLS) design, including poor visibility, turbulent disturbance, carrier air wake, continuously narrow deck motion, and complex sea environment [2]. Hence, developing an ACLS to fully, automatically, and precisely control the aircraft with specific performance has become a significant issue.

Considerable research to address ACLS has been developed. A massive of advanced or intelligent control theories and algorithms have been studied to handle the automatic landing task, such as neural network control [3], adaptive disturbance rejection control [4, 5], backstepping control [6, 7], preview control [8], compensate control based on nonlinear dynamic inverse [9], multivariable adaptive control [10], and prescribed performance control [11]. For example, a PID controller with dynamic inversion for ACLS was designed for longitudinal dynamic flight control [12]. Besides, a nonlinear control law based on the slide-mode control (SMC) technique was designed to address ACLS's robustness [13]. Moreover, the landing trajectory is formulated as a vector field, and a time-varying guidance law was proposed [14]. In addition, a fixed-time flight controller was developed to converge the landing path to the desired profile in a fixed time [15]. Autolanding on the moving CA is very complex due to the nonlinearity, multivariable coupling, parametric uncertainty CA dynamics, and restricted high performance for landing control.

The prescribed performance control (PPC) was first proposed by Bechlioulis and Rovithakis to guarantee transient performance [16]. The essence of PPC is to restrict the tracking error within a specific profile addressing the transient performance. The convergence speed, overshoot, undershoot, and damping ratio should be strictly disciplined. PPC focuses on formulating and integrating prescribed performance in the control design process. For instance, an integral prediction error term was introduced to eliminate the steady-state error [17]. A fuzzy logic system was

addressed for finite-time stability with PPC [18]. Besides, a robust integral of the sign of the error (RISE) term was incorporated to reject the fuzzy logic system approximation errors and external disturbances [19]. In addition, an adaptive decentralized PPC problem for a class of large-scale nonlinear systems was discussed [20]. The PPC strategy was introduced as a practical approach to address the closed-loop performance under specific uncertainty or nonlinearity [21, 22]. The transfer function's pole location drives the closed-loop system's dynamics. Hence, the prescribed performance may be represented as the restriction of pole location in a complex plane.

Guardian maps were introduced as a unifying approach for stability analysis of parameterized families of matrices or polynomials [23]. A monoparametric pseudo-polynomial family is defined by a guardian map to define the maximal stability interval for linear time-invariant fractional-order initialized systems [24]. Guardian maps provide an analytic approach to restrict the poles' location of closed-loop systems. Hence, any closed-loop performance related to the poles' location can be prescribed by guardian maps. Herein, the restriction of poles' location is regarded as the generalized stability. Therefore, flying quality requirements can be represented by the guardian map approach [25].

The application of guardian maps consists of two aspects. The first is to define the boundary of the parametric system with prescribed generalized stability, including control and plant parameters. An analytical approach has been proposed based on guardian maps for stability margin in aircraft design [26]. The second is to design the adaptive law for parameter-varying. The highly nonlinear aero-engine control problem was solved with the LPV/PI control based on guardian maps [27]. Moreover, guardian maps can be utilized in wide-scale nonlinear systems to address scheduling or switching algorithms [28, 29]. Besides, the guardian maps can be integrated into the adaptive control structure to maintain asymptotic convergence [30].

The guardian map approach's superiority lies in directly identifying the stability region. It identifies the performance boundaries with a suitable initial solution [31]. A sufficient condition for determining the performance margin was presented [32]. The guardian map approach is more concise and efficient than the pole-placement approach. Moreover, it can directly limit the feasible range of parameters with a small amount of computation. One- and two-parameter stability problems have been proposed with the analytical solution. In contrast, the multiparameter stability problem has been solved with a numerical approach for solving the null space of guardian maps.

The main contributions of the work are summarized as follows. First, the closed-loop performance is transformed to the pole location of the linearized system, whereas the system's nonlinearity is represented as a shift of pole location. A prescribed performance control method is proposed using the formulated guardian maps for the closed-loop system. Guardian map theory provides a concise approach to identifying the boundary of parameters where the performance degradants. Second, a control-gain design strategy is proposed to prevent performance degradation. Moreover, a velocity-adaptive PPC for CA is developed to validate the proposed approach. The Lyapunov function defines the convergence envelope to ensure the prescribed performance. The convergence envelope is equivalent to the time constant and damping ratio. The Lyapunov function restricts the response from the aspect of energy, whereas the guardian maps approach from the poles' distribution.

The remainder of the paper is organized as follows. The basic principles of guardian map theory are briefly introduced in Section 2. The longitudinal dynamic model of a CA and a velocity-based linear parameter-varying modeling method are described in Section 3. Section 4 presents the process of the adaptive prescribed performance control method. Simulation results and the conclusion come at last.

2. Guardian Maps for Generalized Stability

2.1. Preliminary. The guardian maps were introduced as a unifying approach for studying the generalized stability of parameterized families of matrices or polynomials [23]. A matrix's generalized stability is defined as the open subset Ω in the complex plane containing all matrix eigenvalues. The matrices' set with Ω is expressed as

$$S_\Omega = \{A \in R^{n\times n}; \lambda(A) \subset \Omega\}, \tag{1}$$

where $\lambda(A)$ represents the set of eigenvalues of matrix A. A matrix in the S_Ω is regarded as Ω-stable.

The guardian function ν maps an n-order matrix to a scalar. Let ∂S_Ω indicates the boundary of S_Ω. If the following condition holds, ν is a guardian map of S_Ω.

$$\nu(A) = 0 \Longleftrightarrow A \in \partial S_\Omega. \tag{2}$$

The necessary and sufficient condition (2) implies that the range of the guardian map of genialized stability Ω is polarity-invariant and vanishes on the boundary of Ω. Hence, it provides a comprehensive application for generalized stability analysis for parametric families of matrices. For instance, let a matrix $A(r)$ depend continuously on r, where $r = [r_1, r_2, \cdots, r_k]^{\mathrm{T}} \in R^k$ be a parameter vector. Given the specific stability described as Ω and the corresponding guardian map ν_Ω, the stability range for r can be defined by solving the null space of ν_Ω.

The preliminary generalized stability regions are defined as half-plane, conic sector, and circle, as shown in Figure 1. The formulations of those guardian maps have been proposed.

$$\begin{aligned}
\nu_\sigma(A) &= \det\left(A \odot I - \sigma I \odot I\right) \det\left(A - \sigma I\right),\\
\nu_\zeta(A) &= \det\left[A^2 \odot I + \left(1 - 2\zeta^2\right) A \odot A\right] \det\left(A\right),\\
\nu_\omega(A) &= \det\left(A \odot A - \omega^2 I \odot I\right) \det\left(A^2 - \omega^2 I\right),
\end{aligned} \tag{3}$$

where $\odot$ denotes the bialternate product [33].

The guardian maps for these preliminary regions provide the basis to generate a new region. Any region represented by the intersection, union, or inverse of these

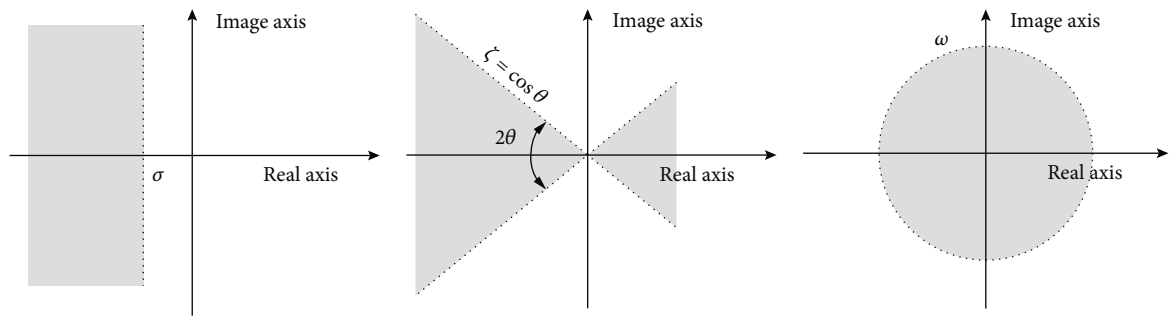

(a) shifted half-plane at σ (b) Sector with θ (c) Circle with radius ω

Figure 1: Preliminary regions Ω.

primary regions has an analytic guardian map formulated as the product of the above functions. The transient performance, such as rise time, damping ratio, and natural frequency, is related to these classic domains, whereas the steady performance, such as steady-state error, cannot be represented as the location of poles. Hence, guardian maps can only address the transient performance of flight control systems in terms of generalized stability.

3. Model Description of Carrier-Based Aircraft

A nonlinear mathematical model of the F/A-18 Hornet aircraft is presented to analyze linear and nonlinear flight control systems. Herein, a reduced-complexity curve fitting model (CFM) is applied to carrier-based aircraft (CA) [34].

Control surfaces for the conventional F/A-18 Hornet aircraft are defined as ailerons, elevators, rudders, leading edge flaps, and trailing edge flaps. The leading and trailing edge flaps provide additional lift during takeoff and landing. Hence, the control analysis and modeling do not consider these control effectors. Only the symmetric elevator δ_{ele} and throttle ϕ are regarded as active control inputs for the studies performed in this paper.

This longitudinal dynamic model derived from Lagrange's equations is formulated as follows:

$$\begin{aligned}
\dot{V} &= \frac{T\cos\alpha - D}{m} - g\sin\gamma,\\
\dot{\alpha} &= -\frac{L + T\sin\alpha}{mV} + \frac{g}{V}\cos\gamma + q,\\
\dot{q} &= \frac{M}{I_{yy}},\\
\dot{\theta} &= q,\\
\dot{h} &= V\sin\gamma,\\
\dot{r} &= V\cos\gamma.
\end{aligned} \tag{4}$$

The nomination of symbols may refer to the nomenclature. The acting forces and moments are calculated using aerodynamic coefficients as follows:

Table 1: Parameters of the CA model.

No.	Parameter	Nomination	Value	Unit
1	Total length	L	17	m
2	Center of gravity	x_{CG}/L	22	%
3	Reference area	S	37	m^2
4	Mean aerodynamic chord	c	3.51	m
5	Mass	m	15097	kg
6	Inertia	I_{yy}	205125	$\text{kg}\cdot\text{m}^2$

$$\begin{aligned}
L &= \bar{q}SC_L,\\
D &= \bar{q}SC_D,\\
M &= \bar{q}ScC_m,
\end{aligned} \tag{5}$$

where $\bar{q}$ represents the dynamic pressure. Table 1 provides the parameters of the CA model [34].

The closed-form formulation of the aerodynamic model is fundamental for stability analysis. Hence, the curve fitting model (CFM) is formulated using the least-square method. The CFM of aerodynamic coefficients under the zero-sideslip assumption is prepared as follows. The parameters in the CFM may refer to Tables 2–4.

$$\begin{aligned}
C_L(\alpha, \delta_{\text{ele}}) &= C_L^{\alpha^3}\alpha^3 + C_L^{\alpha^2}\alpha^2 + C_L^{\alpha}\alpha + C_L^0\\
&\quad + \left(C_L^{\alpha^3\delta}\alpha^3 + C_L^{\alpha^2\delta}\alpha^2 + C_L^{\alpha\delta}\alpha + C_L^{\delta}\right)\delta_{\text{ele}},
\end{aligned}$$

$$\begin{aligned}
C_D(\alpha, \delta_{\text{ele}}) &= C_D^{\alpha^4}\alpha^4 + C_D^{\alpha^3}\alpha^3 + C_D^{\alpha^2}\alpha^2 + C_D^{\alpha}\alpha + C_D^0\\
&\quad + \left(C_D^{\alpha^3\delta}\alpha^3 + C_D^{\alpha^2\delta}\alpha^2 + C_D^{\alpha\delta}\alpha + C_D^{\delta}\right)\delta_{\text{ele}},
\end{aligned}$$

$$\begin{aligned}
C_m(\alpha, \delta_{\text{ele}}, V, q) &= C_m^{\alpha^2}\alpha^2 + C_m^{\alpha}\alpha + C_m^0 + \left(C_m^{\alpha^2\delta}\alpha^2 + C_m^{\alpha\delta}\alpha + C_m^{\delta}\right)\delta_{\text{ele}}\\
&\quad + \left(C_m^{\alpha^3 q}\alpha^3 + C_m^{\alpha^2 q}\alpha^2 + C_m^{\alpha q}\alpha + C_m^{q}\right)\frac{c}{2}\frac{q}{V}.
\end{aligned} \tag{6}$$

Table 2: Parameters of CFM for lift coefficient.

Parameter	$C_L^{\alpha^3}$	$C_L^{\alpha^2}$	C_L^{α}	C_L^0	$C_L^{\alpha^3\delta}$	$C_L^{\alpha^2\delta}$	$C_L^{\alpha\delta}$	C_L^{δ}
Values	1.164	-5.425	5.677	-0.020	2.185	-2.698	0.406	0.572

Table 3: Parameters of CFM for the drag coefficient.

Parameter	$C_D^{\alpha^4}$	$C_D^{\alpha^3}$	$C_D^{\alpha^2}$	C_D^{α}	C_D^0	$C_D^{\alpha^3\delta}$	$C_D^{\alpha^2\delta}$	$C_D^{\alpha\delta}$	C_D^{δ}
Values	1.461	-5.734	6.397	-0.199	0.009	-3.858	4.236	-0.274	0.0367

Table 4: Parameters of CFM for pitch moment coefficient.

Parameter	$C_m^{\alpha^2}$	C_m^{α}	C_m^0	$C_m^{\alpha^2\delta}$	$C_m^{\alpha\delta}$	C_m^{δ}	$C_m^{\alpha^3 q}$	$C_m^{\alpha^2 q}$	$C_m^{\alpha q}$	C_m^{q}
Values	-1.29	0.511	-0.087	0.934	-0.324	-0.905	64.72	-68.56	10.99	-4.12

The flight control system of CA focuses on the attitude dynamics or short-period mode in the longitudinal dynamics, which is reformulated based on equation (4):

$$\dot{\mathbf{x}} = \mathbf{f}_a(\mathbf{x}_a, \mathbf{x}_l) + \mathbf{g}_a(\mathbf{x}_l, \mathbf{p})\delta_{ele} \tag{7}$$

where $x_a = [\alpha, q]^T$ and $\boldsymbol{x}_l = [V, \theta]^T$. The linearized state space representation of the nonlinear system (7) is formulated as

$$\begin{bmatrix} \Delta\dot{\alpha} \\ \Delta\dot{q} \end{bmatrix} = \begin{bmatrix} -\dfrac{L_\alpha + T_\alpha \sin\alpha}{V} & -\dfrac{T\cos\alpha}{mV} & 1 \\ M_\alpha & & 0 \end{bmatrix} \begin{bmatrix} \Delta\alpha \\ \Delta q \end{bmatrix} + \begin{bmatrix} -\dfrac{L_\delta}{V} \\ M_\delta \end{bmatrix} \Delta\delta_{ele}. \tag{8}$$

The dimensional derivatives in equation (8) are calculated based on the nondimensional derivatives:

$$\begin{aligned} L_\alpha &= \frac{\bar{q}S}{m} C_{L\alpha}, \\ M_\alpha &= \frac{\bar{q}Sc}{I_{yy}} C_{m\alpha}, \\ L_\delta &= \frac{\bar{q}S}{m} C_{L\delta}, \\ M_\delta &= \frac{\bar{q}Sc}{I_{yy}} C_{m\delta}. \end{aligned} \tag{9}$$

3.1. Adaptive Prescribed Performance Control. The following section presents a velocity-adaptive prescribed performance control methodology based on guardian maps. A classic PI controller structure is adopted in the attitude loop to illustrate the controller design process. The controller parameters are donated as $K = [K_P, K_I]$. The prescribed performance is specified in the time domain: stability margin, damping, or flying quality requirements. All these requirements can be transformed into the restriction of pole location in complex planes using guardian maps.

Table 5: Flying quality boundaries [35].

ζ_{sp}	ω_{sp}	$\omega_{BW\theta}$
0.35~1.30	>0.87 rad/s	>1.5 rad/s

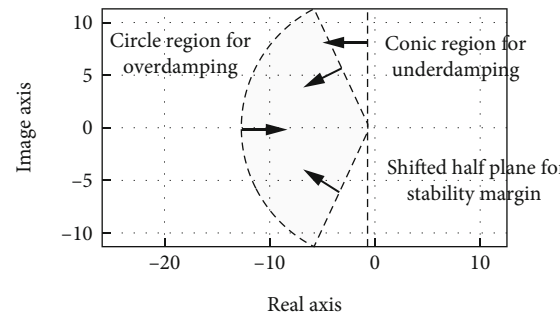

Figure 2: Generalized stability region for prescribed performance.

3.1.1. Generalized Stable Region for Prescribed Performance. The flying quality (FQ) criteria declare the performance boundary of dynamic responses. The short-period mode focuses on ζ_{sp}, ω_{sp}, and $\omega_{BW\theta}$. These performance specifications can be formulated as generalized stability using the above-introduced classical regions. Boundaries for these criteria are listed in Table 5.

The pole location dominates the short-period polynomial, indicating the information of ζ_{sp} and ω_{sp}. If the roots of the short-period polynomial are denoted as p_1 and p_2, then ζ_{sp} and ω_{sp} can be expressed by the pole's location as follows:

$$\begin{aligned} \zeta_{sp} &= \frac{p_1 + p_2}{2\sqrt{p_1 p_2}}, \\ \omega_{sp} &= \sqrt{p_1 p_2}. \end{aligned} \tag{10}$$

The lower bound on the damping ratio contains the underdamped response, indicating a pair of complex poles in the short-period mode. The upper bound on the damping

Input: the initial parameter $\boldsymbol{p}_0$, and the tolerance of parameter shift *tole*
Initialize the current parameter and the shift of parameter: $\boldsymbol{p}_c = \boldsymbol{p}_0$, $d_p = 1$.
While $d_p > tole$
  Initial the following trial parameter: $\boldsymbol{p}_n = \boldsymbol{p}_c$.
  For i = 1:dim($\boldsymbol{p}_n$)
    Calculate the null space of the i-th dimension based on $\boldsymbol{p}_n$, and obtain the feasible region $[p_l(i), p_u(i)]$.
    Update the value of the i-th dimension parameter as the middle value in the feasible region: $\boldsymbol{p}_n(i) = \text{mean}(p_l(i), p_u(i))$.
  End
  Calculate the shift of the updated parameter: $d_p = \|\boldsymbol{p}_n - \boldsymbol{p}_c\|_2$.
  Update the current parameter: $\boldsymbol{p}_c = \boldsymbol{p}_n$;
end
Output: the current parameter $\boldsymbol{p}_c$.

Algorithm 1: Algorithm for seeking the center of the multiparametric feasible region.

ratio addresses the overdamping response, where the two poles of short-period mode are located at the real axis. Hence, the damping ratio $\zeta_{sp} < 1.3$ requirement implies that $0.22 < p_1/p_2 < 4.54$.

The transformation of the prescribed performance to the generalized stable region in the complex plane is shown in Figure 2. The stability margin is defined as the minimum distance from closed-loop poles to the imaginary axis, which can be represented as a generalized stable region Ω_σ. The underdamped ratio, described as an overshoot of step response, is directly related to the generalized stable region Ω_ζ. Ω_ω restricts the maximum distance from the poles to the origin, which can indicate the requirement for overdamping ratio.

The guardian map approach provides a potent tool for parametric stability analysis. It extends Hurwitz's stability to any desired region expressed by the guardian maps in a complex plane, which affords the performance analysis (generalized stability) for a parametric system.

3.1.2. Gain Scheduling for Velocity-Adaptive PPC. This work is aimed at determining whether the controller parameters can maintain the closed-loop prescribed performance as the velocity variance. If not, how to make adjustments? According to guardian map theory, all parameters in the subspace bounded by the null space share the same generalized stable region defined by it. Since the prescribed performance has been represented as the combination of the classic generalized stable region of guardian maps, one can calculate the corresponding function's null space and determine the parameter's boundary remains prescribed performance. Moreover, one can propose a parameter-scheduled strategy to design a parameter corridor to maintain the specified version. Herein, the velocity is regarded as a scheduled parameter to create the corridor of controller parameters.

The linearized system of the short-period dynamics can be featured the velocity V and denoted as

$$\begin{aligned} \Delta\dot{\mathbf{x}} &= A(V)\Delta x + b(V)\Delta\delta_{\text{ele}}, \\ \Delta\delta_{\text{ele}} &= \left(\frac{K_I}{s} + K_P\right)(q_c - q). \end{aligned} \tag{11}$$

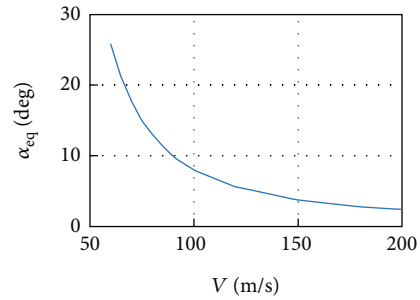

Figure 3: The trimmed AOA with velocity.

The state matrix of the closed-loop system is denoted as $A_c(V, K)$ for Equation (11), where $\underline{K} = [K_I, K_P]^T$. Prescribed performance relates to the damping ratio, and bandwidth has been transformed to the generalized stability domain as a combination of preliminary regions.

A guardian map for the specific generalized stability domain is then formulated as

$$\nu_\Omega[A_c(V,K)] = \nu_\sigma[A_c(V,K)]\nu_\zeta[A_c(V,K)]\nu_\omega[A_c(V,K)]. \tag{12}$$

The guardian map approach identifies the controller gain boundary by calculating Equation (12) 's null space.

$$\nu_\Omega[A_c(V_s, K_{\text{null}})] = 0, \tag{13}$$

where K_{null} denotes the null space, the dimension of which is one less than the design space. V_s is the scheduled parameter, which can be regarded as a section in the design space.

Theoretically, any parameter in the connected region shares the same prescribed performance. However, the parameter near the boundary indicates that the closed-loop performance is most critical. Hence, a parameter selection strategy should be proposed to prevent boundary situations. In this paper, a central policy is adopted to determine the parameter; that is, the location of the parameter is at the

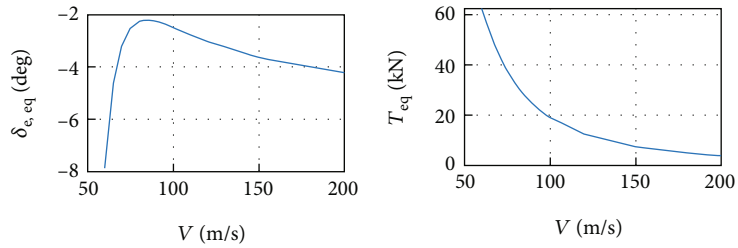

(a) Deflection of elevator (b) Thrust

Figure 4: The trimmed inputs with velocity.

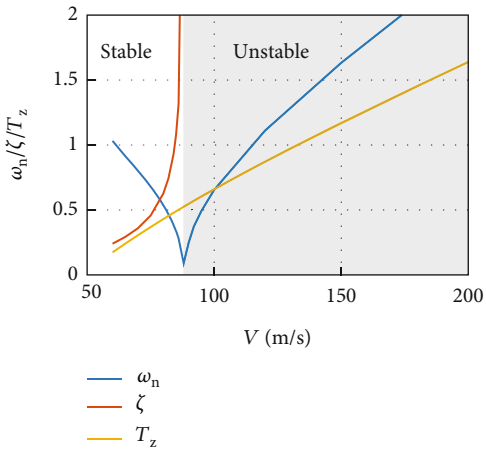

Figure 5: The dynamic characteristic of CA with velocity.

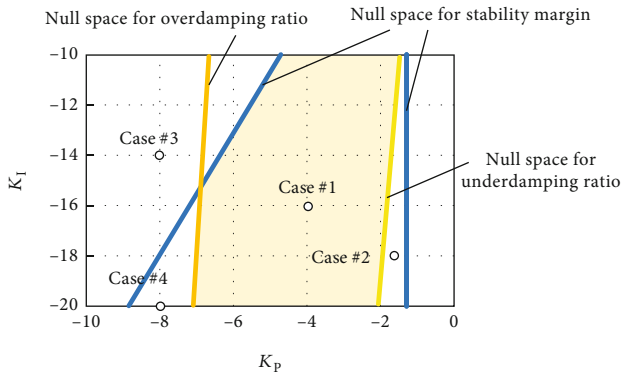

Figure 6: Null space of parameter space for the prescribed performance based on guardian maps.

middle position in the feasible range. A multiparametric center-seeking algorithm is proposed in Algorithm 1.

4. Simulation and Discussion

This section applies the reduced-complexity linear model to design the velocity-adaptive PPC and a nonlinear simulation model (SM) for numerical simulation. The flight conditions are $h = 100$ m and $V = 80$ m/s~200 m/s.

4.1. Dynamics of Carrier-Based Aircraft. The dynamics of CA are first examined. The trimmed conditions with velocity are shown in Figures 3 and 4. The stall velocity of CA is about 60 m/s. Figure 3 shows the trimmed angle of attack (AOA) tendency with an increased velocity at a fixed altitude $h = 100$ m. The AOA dramatically increases as the speed drops to 100 m/s. Besides, the trimmed deflection angle of the elevator and thrust with velocity are shown in Figure 4.

The thrust trend coincides with AOA, whereas the elevator deflection increases first and then decreases. The cause of the phenomenon is the change in the stability of the plant, which is shown in Figure 5.

The damping ratio, the natural frequency of short-period mode, and the time constant of zeros in the pitch channel are shown in Figure 5. The short-period mode of CA is unstable as the speed is above 85 m/s. The open-loop dynamics change dramatically as the velocity decreases, challenging a flight control system.

4.2. Attitude Control with Prescribed Performance. The prescribed performance control based on guardian maps is formulated in Section 4. Herein, we present an example to illustrate the validation of the proposed prescribed performance control based on guardian maps. The stability margin is set to be -0.87, the overshoot of pitch response is 20%, and the maximum damping ratio is 1.7. Guardian map with prescribed performance is formulated as mentioned in Section 4, and the null space in the control parameter space is shown in Figure 6. The design space is split into six subspaces, and the performance boundaries are defined as the null space illustrated in different colors. Guardian map theory indicates that parameters in the same connected subspace share the same generalized stability. Hence, we examine four cases for validation, as shown in Figure 6.

The pitch responses of the closed-loop system with specific controller parameters, as shown in Figure 6, are presented in Figure 7. The prescribed performance is shown in red as the stability margin and underdamped ratio, whereas the overdamping ratio cannot be directly marked in the time domain.

Simulation results in Figure 7 show that the closed-loop system with the controller in case #1 satisfies the prescribed performance. However, the overshoot of pitch response for the closed-loop system with the controller in case #2 exceeds the restriction. Moreover, controller parameters in case #2 cross over the boundary delineated by the null space of guardian maps. As for case #3 and case #4, the time responses are beyond the requirements for the overdamping

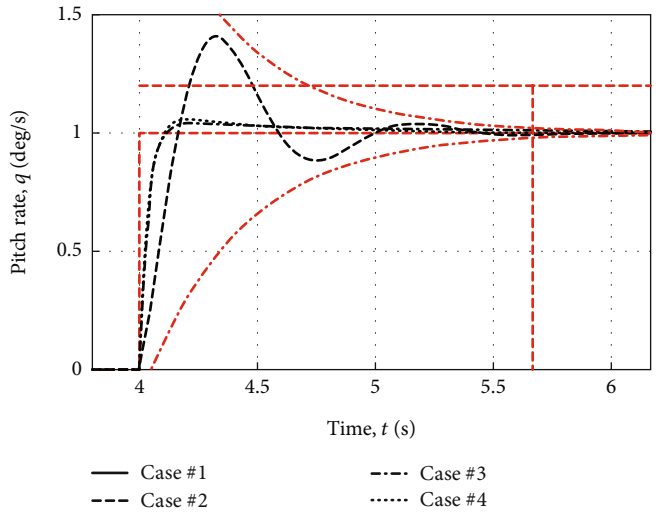

Figure 7: Validation of guardian map approach to prescribed performance.

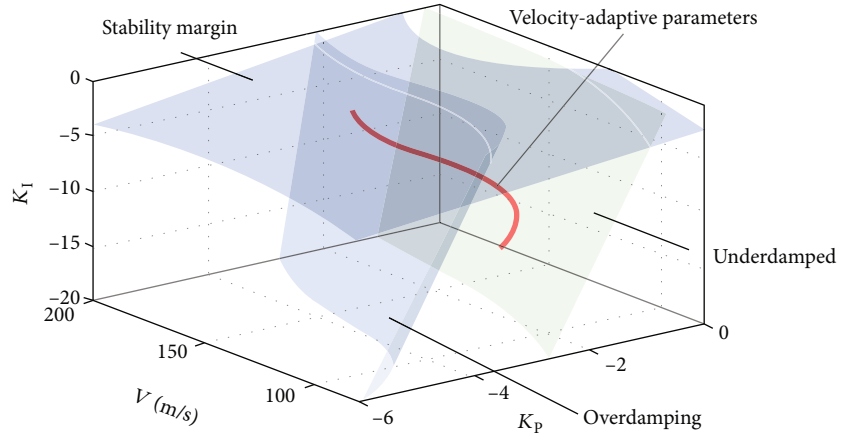

Figure 8: Velocity-scheduled corridor of control parameters with prescribed performance.

ratio. In addition, the time response is affected by zero dynamics, which can also be restricted by the specific region using guardian maps. In this paper, we focus on the pole dynamics with varying velocities. Flight control design and simulation results are presented in the following subsection.

4.3. Validation for VA-PPC. The pitch control of CA is assumed to be a PI controller. The dynamics of the closed-loop system are determined by the controller parameters K_P and K_I. In addition, the dynamics of open-loop vary dramatically as speed changes. Three parameters drive the dynamics of the closed-loop system, and the dimension of null space of guardian maps is two, which are surfaces shown in Figure 8. Considering the control saturation, we assume that the maximum gain of the controller is 20. The multi-parametric center-seeking algorithm is applied to determine K_P and K_I for each velocity-scheduled section, listed in Table 6. The path of controller parameters in the velocity-scheduled corridor is approximated by the polynomial fitting of sectional parameters in Table 6 and shown as the black line in Figure 8.

Table 6: Centre control parameters of velocity-scheduled section.

V (m/s)	80	100	120	150	200
K_P	-3.56	-2.50	-2.05	-1.99	-1.51
K_I	-8.95	-8.40	-8.12	-7.91	-7.85

Pitch responses at different velocities are shown in Figure 9 with velocity-adaptive PPC. Simulation results indicate that the dynamic pitch response satisfies the prescribed performance concerning the velocity variance. In particular, the damping characteristic shows consistency, which validates the effectiveness of prescribed performance control.

In addition, we examine the boundary conditions to check the necessity of a velocity-adaptive controller. Herein, we set the controller parameters obtained at $V = 200$ m/s as a baseline controller and fixed them. Then, the pitch control at $V = 80$ m/s is performed. The two responses are shown in Figure 10. If we keep the same controller parameter for $V = 80$ m/s, the overshoot of the pitch response will exceed the performance requirement.

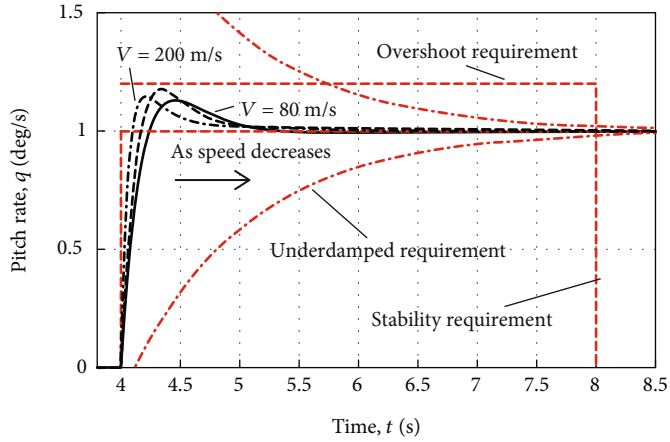

Figure 9: Pitch response of CA with VA-PPC.

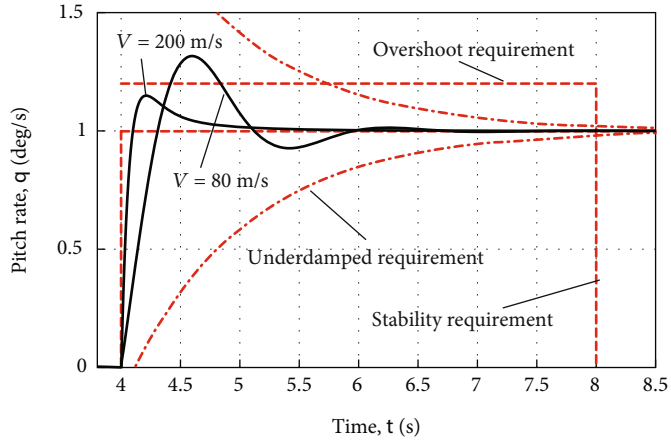

Figure 10: Pitch response of CA for fixed control parameter obtained at $V = 200$ m/s.

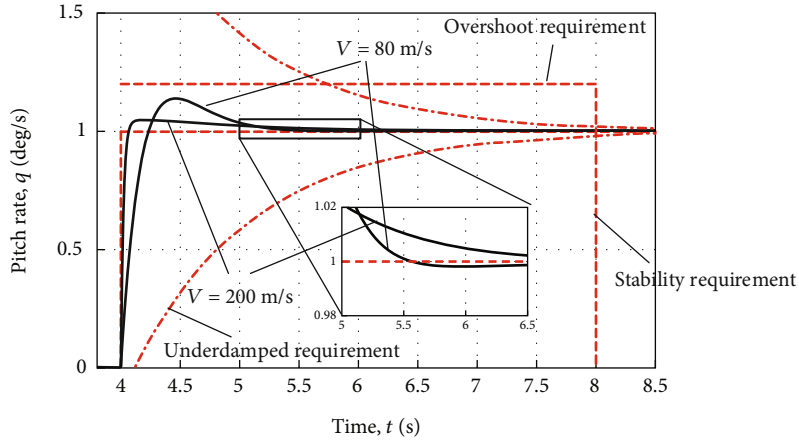

Figure 11: Pitch response of CA for fixed control parameter obtained at $V = 80$ m/s.

Next, we compare the pitch responses for both velocities while the controller parameters are obtained at 80 m/s. Simulation results reveal that the overdamping of pitch response will arise if we do not apply the velocity-adaptive strategy, as shown in Figure 11.

5. Conclusions

This paper proposes a velocity-adaptive prescribed performance control method based on guardian maps. In general, the stability of pitch dynamics for carrier-based aircraft

varies from unstable to stable as speed drops off. Besides, the damping characteristic shows more underdamped. Guardian maps extend Hurwitz's stability to generalized stability revealing the transient performance, which affords the parametric analysis approach to closed-loop performance. A velocity-scheduled control strategy is adopted to maintain the prescribed performance of the damping ratio. Moreover, the appropriate values for controller parameters are generated at the center point, where the average distance to the performance boundary is the farthest. The characteristic polynomial of the transfer function's numerator causes the time response's deviation. Simulation validates the effectiveness of the proposed method. The proposed approach not only defines the appropriate range of control parameter to ensure the prescribed performance but also provides the adaptive law for the scheduling parameter with a simple strategy.

Nomenclature

D: Drag
L: Lift
M: Pitch moment
T: Thrust
V: Velocity
h: Altitude
q: Pitch rate
r: Range
α: Angle of attack
γ: Flight path angle
θ: Pitch angle
ω_{sp}: The natural frequency of the short-period mode
$\omega_{BW\theta}$: Pitch attitude bandwidth
ζ_{sp}: The damping ratio of the short-period mode.

Data Availability

The carrier-based aircraft model data are provided in Tables 2–4.

Conflicts of Interest

The authors declare that there is no conflict of interest regarding the publication of this paper.

Acknowledgments

This work was supported by the Natural Science Foundation of Jiangsu Province for distinguished young scholars (grant number BK20190017) and the National Natural Science Foundation of China (grant numbers 62103187).

References

[1] J. M. Urnes and R. K. Hess, "Development of the f/a-18a automatic carrier landing system," *Journal of Guidance, Control, and Dynamics*, vol. 8, no. 3, pp. 289–295, 1985.

[2] A. L. Prickett and C. J. Parkes, "Flight testing of the F/A-18E/F automatic carrier landing system," in *IEEE Aerospace Conference Proceedings*, pp. 52593–52612, Big Sky, MT, USA, 2001.

[3] M. Lungu and R. Lungu, "Automatic control of aircraft lateral-directional motion during landing using neural networks and radio-technical subsystems," *Neurocomputing*, vol. 171, pp. 471–481, 2016.

[4] X. Wang, X. Chen, and L. Wen, "Adaptive disturbance rejection control for automatic carrier landing system," *Mathematical Problems in Engineering*, vol. 2016, Article ID 7345056, 12 pages, 2016.

[5] Y. Liang, X. Chen, and Z. Xu, "Research on longitudinal landing track control technology of carrier-based aircraft," in *Proceedings of the 32nd Chinese Control and Decision Conference*, pp. 3039–3044, Hefei, China, 2022.

[6] M. Lungu, "Auto-landing of UAVs with variable centre of mass using the backstepping and dynamic inversion control," *Aerospace Science and Technology*, vol. 103, article 105912, 2020.

[7] F. Zheng, Z. Zhen, and H. Gong, "Observer-based backstepping longitudinal control for carrier-based UAV with actuator faults," *Journal of Systems Engineering and Electronics*, vol. 28, no. 2, pp. 322–337, 2017.

[8] S. Jiang, Z. Zhen, J. Jiang, and Z. Yang, "A Preview control scheme for carrier-based aircraft automatic landing," in *2018 37th Chinese Control Conference (CCC)*, pp. 9815–9819, Wuhan, China, 2018.

[9] F. Luo, J. Zhang, P. Lyu, Z. Liu, and W. Tang, "Carrier-based aircraft precision landing using direct lift control based on incremental nonlinear dynamic inversion," *IEEE Access*, vol. 10, pp. 55709–55725, 2022.

[10] Z. Zhen, G. Tao, C. Yu, and Y. Xue, "A multivariable adaptive control scheme for automatic carrier landing of UAV," *Aerospace Science and Technology*, vol. 92, pp. 714–721, 2019.

[11] W. Hu, K. Yong, and M. Chen, "Disturbance interval observer-based carrier landing control of unmanned aerial vehicles using prescribed performance," *Scientia Sinica Informationis*, vol. 52, no. 9, pp. 1711–1726, 2022.

[12] R. Lunge, M. Lungu, and T. L. Grigorie, "Automatic control of aircraft in longitudinal plane during landing," *IEEE Transactions on Aerospace and Electronic Systems*, vol. 49, no. 2, pp. 1335–1350, 2013.

[13] S. Lee, J. Lee, S. Lee et al., "Sliding mode guidance and control for UAV carrier landing," *IEEE Transactions on Aerospace and Electronic Systems*, vol. 55, no. 2, pp. 951–966, 2019.

[14] Z. Guan, Y. Ma, and Z. Zheng, "Moving path following with prescribed performance and its application on automatic carrier landing," *IEEE Transactions on Aerospace and Electronic Systems*, vol. 56, no. 4, pp. 2576–2590, 2020.

[15] Z. Guan, H. Liu, Z. Zheng, M. Lungu, and Y. Ma, "Fixed-time control for automatic carrier landing with disturbance," *Aerospace Science and Technology*, vol. 108, article 106403, 2021.

[16] C. P. Bechlioulis and G. A. Rovithakis, "Robust adaptive control of feedback linearizable MIMO nonlinear systems with prescribed performance," *IEEE Transactions on Automatic Control*, vol. 53, no. 9, pp. 2090–2099, 2008.

[17] S. Hu, X. Ren, and D. Zheng, "Integral predictor based prescribed performance control for multi-motor driving servo systems," *Journal of the Franklin Institute*, vol. 359, no. 16, pp. 8910–8932, 2022.

[18] H. Lv, W. Xiang, and J. Zhu, "Finite time prescribed performance control for uncertain second-order nonlinear systems," *Journal of Mathematics*, vol. 2022, Article ID 7404460, 7 pages, 2022.

[19] Y. Zhou and S. Wang, "Adaptive prescribed performance control for nonlinear robotic systems," *Journal of the Franklin Institute*, vol. 360, no. 2, pp. 1378–1394, 2023.

[20] S. L. Zhu and Y. Q. Han, "Adaptive decentralized prescribed performance control for a class of large-scale nonlinear systems subject to nonsymmetric input saturations," *Neural Computing and Applications*, vol. 34, no. 13, pp. 11123–11140, 2022.

[21] Z. Wu, J. Ni, W. Qian, X. Bu, and B. Liu, "Composite prescribed performance control of small unmanned aerial vehicles using modified nonlinear disturbance observer," *ISA Transactions*, vol. 116, pp. 30–45, 2021.

[22] Z. He, J. Hu, Y. Wang, J. Cong, L. Han, and M. Su, "Sample entropy based prescribed performance control for tailless aircraft," *ISA Transactions*, vol. 131, pp. 349–366, 2022.

[23] L. Saydy, A. Tits, and E. Abed, "Guardian maps and the generalized stability of parametrized families of matrices and polynomials," *Mathematics of Control, Signals, and Systems*, vol. 3, no. 4, pp. 345–371, 1990.

[24] J. A. López-Rentería, B. Aguirre-Hernández, and G. Fernández-Anaya, "A new guardian map and boundary theorems applied to the stabilization of initialized fractional control systems," *Mathematicsl Methods in the Applied Sciences*, vol. 45, no. 12, pp. 7832–7844, 2022.

[25] D. Sausslé, L. Saydy, and O. Akhrlf, "Longitudinal flight control design with handling quality requirements," *Aeronautical Journal*, vol. 110, no. 1111, pp. 627–637, 2006.

[26] H. Lei, B. Chen, Y. Liu, and Y. Lu, "Guardian map approach to feasible range of static stability margin of hypersonic flight vehicles with input saturation," *International Journal of Aerospace Engineering*, vol. 2020, Article ID 8895324, 11 pages, 2020.

[27] Y. Qian, Z. Ye, H. Zhang, and L. Zhou, "LPV/PI control for nonlinear aeroengine system based on guardian maps theory," *IEEE Access*, vol. 7, pp. 125854–125867, 2019.

[28] D. Xiao, M. Liu, Y. Liu, and Y. Lu, "Switching control of a hypersonic vehicle based on guardian maps," *Acta Astronautica*, vol. 122, pp. 294–306, 2016.

[29] B. Chen, Y. Liu, H. Lei, H. Shen, and Y. Lu, "Ascent trajectory tracking for an air-breathing hypersonic vehicle with guardian maps," *International Journal of Advanced Robotic Systems*, vol. 14, no. 3, 2017.

[30] Y. Chihabi and S. Ulrich, "Hybrid guardian map-based adaptive control of spacecraft formation flying on highly elliptical orbits in the restricted three-body problem," *Acta Astronautica*, vol. 180, pp. 370–385, 2021.

[31] D. Saussié, L. Saydy, O. Akhrif, and C. Bérard, "Gain scheduling with guardian maps for longitudinal flight control," *Journal of Guidance, Control, and Dynamics*, vol. 34, no. 4, pp. 1045–1059, 2011.

[32] B. Chen, J. Chen, Y. Liu, H. Lei, and S. Jia, "Guardian maps based robust stability analysis with applications in flight control of hypersonic vehicles," *Aerospace Science and Technology*, vol. 106, p. 106208, 2020.

[33] J. W. Brewer, "Kronecker products and matrix calculus in system theory," *IEEE Transactions on Circuits and Systems*, vol. 25, no. 9, pp. 772–781, 1978.

[34] A. Chakraborty, *Linear and Nonlinear Analysis of Susceptibility of F/A-18 Flight Control Laws to the Falling Leaf Mode T*, University of Minnesota, 2011.

[35] MIL-STD-1797A, *Flying Qualities of Piloted Aircraft*, Department of Defense, USA, 1997.